Check for updates

Dehydrogenative oxidation of hydrosilanes using gold nanoparticle deposited on citric acid-modified fibrillated cellulose: unveiling the role of molecular oxygen†

Butsaratip Suwattananuruk,[a] Yuta Uetake, ✱[a,b] Rise Ichikawa,[c] Ryo Toyoshima,[c] Hiroshi Kondoh [c] and Hidehiro Sakurai ✱[a,b]

Efficient and environmentally friendly synthesis of silanols is a crucial issue across the broad fields of academic and industrial chemistry. Herein, we describe the dehydrogenative oxidation of hydrosilane using a gold nanoparticle catalyst supported by fibrillated citric acid-modified cellulose (F-CAC). Au:F-CAC catalysts with various particle sizes (1.7 nm, 4.9 nm, and 7.7 nm) were prepared using the *trans*-deposition method, a technique previously reported by our group. These catalysts exhibited significant catalytic activity to produce silanols with high turnover frequency (TOF) of up to 7028 h^{-1}. Recycling experiments and transmission electron microscopy (TEM) observation represented the high durability of Au:F-CAC under the reaction conditions, allowing kinetic studies on size dependency. Mechanistic studies were conducted, including isotope labelling experiments, kinetics, and various spectroscopies. Notably, the near ambient pressure X-ray photoelectron spectroscopy (NAP-XPS) of the model catalyst (Au:PVP) revealed the formation of catalytically active cationic Au sites on the surface through the adsorption of molecular oxygen, providing a new insight into the reaction mechanism.

1. Introduction

Considering the growing demand for silicon-based compounds and materials, silanols serve diverse purposes including excellent building blocks for silicon-based polymeric materials,[1] pharmacological functional groups,[2] coupling reagents[3] and protecting groups[4] in organic synthesis. Traditionally, silane oxidation required a stoichiometric amount of oxidants, inevitably producing a stoichiometric amount of by-products.[5–10] Therefore, catalytic dehydrogenative oxidation of hydrosilanes has garnered attention in the context of its nontoxic attributes as a reactant, with hydrogen being the only by-product, rendering these processes clean and environmentally benign.[11–13] Among them, gold nanoparticles (AuNPs) are well-known catalysts for aerobic oxidation

reactions.[14–19] Besides, from the first report of the AuNP-catalysed oxidation of hydrosilanes under aerobic conditions by Kaneda *et al.*,[14] various AuNP catalysts stabilised on solid-supports such as hydroxyapatite (HAP),[15] carbon nanotubes (CNTs),[20–22] cellulose,[23] and manganese oxide (MnO$_2$)[24,25] have been investigated for the oxidation of hydrosilane. These reports exhibited that solid supports play an important role in catalytic activity; therefore, developing novel support is crucial to enhancing catalytic activity.

In the context of promoting sustainable and environmentally friendly science, the use of cellulose-based materials, which are abundant in nature, holds great potential. We have established an easy and scalable method for fabricating citric acid-modified cellulose (F-CAC), easily defibrated into a fluffed nanostructure using a commercially available mixer.[26,27] The fluffed nanostructure and high tolerance against organic solvents of F-CAC make it suitable as a heterogeneous catalyst for reaction in organic solvents. Our earlier work demonstrated the size-selective preparation of Au:F-CAC catalysts through the *trans*-deposition method (Fig. 1).[28–30] Using the size-selectively prepared Au:PVP(K-15) (PVP: poly(*N*-vinyl-2-pyrrolidone)),[31,32] Au:F-CAC with various particle sizes (1.7–8.2 nm) can be prepared, enabling investigation of size effects. The thus-prepared Au:F-CACs have been applied to the oxidation of alcohols[30] and intramolecular cyclisation reaction of amines, showing

*[a]Division of Applied Chemistry, Graduate School of Engineering, Osaka University, 2-1 Yamadaoka, Suita, Osaka 565-0871, Japan.
E-mail: uetake@chem.eng.osaka-u.ac.jp, hsakurai@chem.eng.osaka-u.ac.jp*
[b]Innovative Catalysis Science Division, Institute for Open and Transdisciplinary Research Initiatives (ICS-OTRI), Osaka University, 2-1 Yamadaoka, Suita, Osaka 565-0871, Japan
[c]Department of Chemistry, Faculty of Science and Technology, Keio University, Kohoku-ku, Yokohama 223-8522, Japan
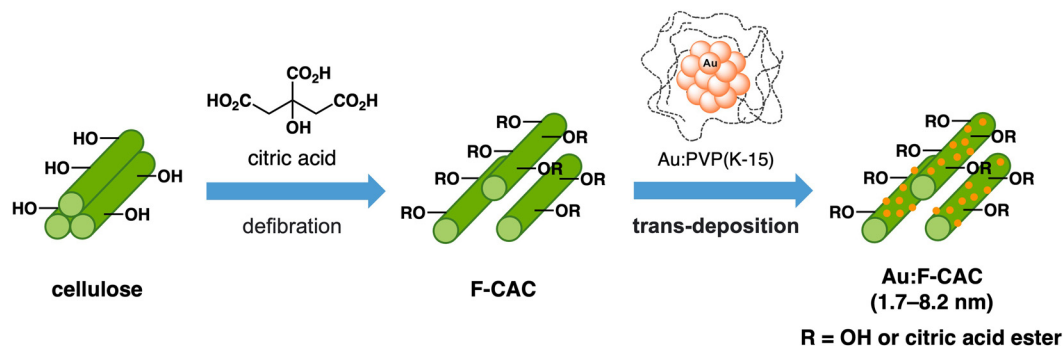†Electronic supplementary information (ESI) available. See DOI: https://doi.org/10.1039/d4nr01184h

Fig. 1 Citric acid-modification of cellulose and size-selective preparation of Au:F-CAC.

good catalytic activity.[33] Besides, AuNPs in Au:F-CAC are stable enough under the reaction conditions, possibly due to the benefits of introduced coordinative carboxy groups, allowing the size-selective preparation and recycling.

In this study, we investigated the catalytic activity of Au:F-CAC on the dehydrogenative oxidation of hydrosilane. The size-selectively prepared Au:F-CAC catalysts were subjected to kinetic studies, unveiling the size effect that has not been considered. In addition, the labelling experiments and the detailed spectroscopic analyses of the model AuNP catalyst using near-ambient pressure X-ray photoelectron spectroscopy (NAP-XPS) and solution-state X-ray absorption spectroscopy (XAS) were conducted to uncover the effect of molecular oxygen on the AuNP under aerobic conditions.

2. Experimental section

Preparation of Au:F-CAC catalyst

Au:PVP(K-15) and Au:PVP(K-30) were prepared according to the literature procedure.[31,32] F-CAC[33] and Au:F-CAC[30,33] were prepared according to the literature procedure. In a reaction tube (φ = 3 cm) equipped with a magnetic stir bar, Au:PVP(K-15) (5.1×10^{-3} mmol of Au) and F-CAC (600 mg) were mixed in EtOH (30 mL), and then the pH was adjusted to 4 using aqueous hydrochloric acid solution (0.1 mol L^{-1}). After stirring at 27 °C (1300 rpm) for 90 min, the solid was separated from the supernatant by centrifugation (7500 rpm) at room temperature and washed with ethanol (*ca.* 30 mL × 3). The remaining powder was dried under vacuum at 45 °C for 12 h to afford Au:F-CAC (1.7×10^{-3} wt%).

General procedure for dehydrogenative oxidation of hydrosilane

To a reaction tube equipped with a magnetic stir bar, Au:F-CAC, hydrosilane (0.50 mmol), water, and solvent (3 mL) were added. The mixture was stirred at 27 °C under an ambient atmosphere. After stirring for a specific period, the catalyst was removed by filtration and washed with diethyl ether (*ca.* 5 mL × 3). The filtrate was concentrated under reduced pressure. To the residue was added 1,1,2,2-tetrachlor-oethane (52.7 μL, 0.50 mmol) and CDCl$_3$ (*ca.* 1 mL), and then ^{1}H NMR analysis was conducted using a portion of this solution. The yields were determined by comparison of an integrated value of the peak that corresponds to a proton of silanol with that corresponding to two protons of 1,1,2,2-tetrachloroethane (δ 5.98 ppm).

Recycling run experiment

To a reaction tube equipped with a magnetic stir bar was added Au:F-CAC (0.01 atom%), **1a** (0.50 mmol), water (400 mol%), and THF (3 mL). The mixture was stirred at 27 °C under an ambient atmosphere. After stirring for 5 h, the catalyst was removed by filtration and washed with diethyl ether (*ca.* 5 mL × 3). The spent catalyst was dried at 45 °C under reduced pressure for 12 h, and this was used for the next recycling run.

Near ambient pressure X-ray photoelectron spectroscopy experiment of Au:PVP under oxygen/water atmosphere

The near ambient pressure X-ray photoelectron spectroscopy (NAP-XPS) experiments were performed at the BL13B beamline of photon factory (PF) equipped with an APPLE II type undulator[34] under the ring-conditions of 2.5 GeV and 450 mA. X-ray beam energy was tuned to be 630 eV by a Monk-Gillieson-type monochromator.[35] NAP-XPS data was collected at Au 4f and Si 2p core levels with constant analyser energy (CAE) mode with the energy step size of 0.05 eV at room temperature. The binding energy was corrected using the Si 2p$_{3/2}$ signal of a Si substrate to 99.1 eV. The spectra were normalised to exclude the attenuation caused by the introduced gases.

A silicon substrate (P-type, low conductivity, Si(100) facet, Nilaco Co., SI-500440, *ca.* 10 mm × *ca.* 10 mm × 0.5 mm) was cleaned by ultrasound irradiation in ethanol for 15 min and dried under ambient atmosphere. 6.8 mg of Au:PVP(K-30) was dissolved in ethanol (20 mL) using a volumetric flask to prepare 3.0 mmol L^{-1} Au:PVP(K-30) solution. 0.1 mL of the solution was diluted with 0.9 mL ethanol to afford 0.3 mmol$_{PVP}$ L^{-1} Au:PVP(K-30) solution. 5 μL of the Au:PVP(K-30) solution (0.3 mmol$_{PVP}$ L^{-1}) was applied on a Si substrate. After drying, the sample was attached to a sample holder. The sample holder was fixed on a sample bank, and

then this was connected to a linear and rotatable manipulator. After the pressure in the load-lock chamber reached less than 1×10^{-7} Torr, the sample was transferred to a main chamber. XPS data were collected under the pressure of 6.8×10^{-9} Torr. Then, oxygen gas was slowly introduced to the main chamber from a gas cylinder connected through a variable leak valve. After the pressure of the main chamber reached 0.1 Torr, NAP-XPS experiments were performed under an oxygen atmosphere. H_2O was purified by the freeze–thaw-pumping method and slowly introduced by a variable leak valve to the main chamber. After the pressure of the main chamber reached 0.2 Torr (p_{oxygen} = 0.1 Torr, p_{water} = 0.1 Torr), NAP-XPS experiments were performed under the oxygen/water atmosphere.

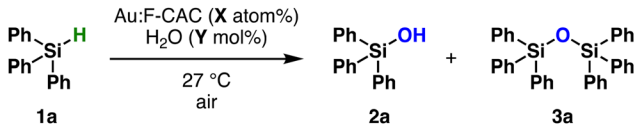### Solution-state X-ray absorption spectroscopy of Au:PVP in water

Au L_3-edge X-ray absorption spectroscopy (XAS) experiments were performed at the BL14B2 beamline of SPring-8 using Si (111) double-crystal monochromatised synchrotron radiation under the ring-conditions of 8.0 GeV and 100 mA. All experiments were carried out using the fluorescent method with quick scan technique (QXAFS) at room temperature, otherwise noted. Ionisation chambers were used to measure the intensities of the incident (I_0) and transmitted (I_1) X-ray. X-ray fluorescence was monitored using a 19-element Ge solid-state detector (SSD). XAS analysis was conducted using the Demeter package, a comprehensive system for processing and analysing XAS data.[36–38] Background removal and normalisation of raw data were performed using the cubic spline method using Athena software. E_0 was defined as photon energy at the absorption edge where $\mu T = 0.5$ in the normalised XAS spectrum. E_0 values of Au foil were set to 11919 eV for photon energy calibration. Reference samples (Au foil and Au_2O_3) were measured using the transmission method.

Au:PVP(K-30) was dissolved in H_2O to prepare 8.0 $mmol_{Au}$ L^{-1} solution. The solution was introduced in a polyethylene bag and subjected to an XAS experiment. Then, the solution was bubbled with N_2 gas at the flow rate of 60 mL min^{-1} for 15 min to degas the dissolved oxygen. After sealing, the XAS experiment was again conducted.

3. Results and discussion

The Au:F-CAC catalyst with the particle size of 1.7 ± 0.8 nm (1.7×10^{-3} wt%) was prepared according to the reported method,[30] and the dehydrogenative oxidation of hydrosilane was investigated using triphenylsilane (**1a**) as a substrate. In the presence of Au:F-CAC (0.5 atom%) and H_2O (1000 mol%) in n-hexane, the oxidation of hydrosilane proceeded to give triphenylsilanol (**2a**) in 58% yield after 15 min (Table 1, entry 1). Hexaphenyldisiloxane (**3a**) was not detected. The use of polar solvents, such as EtOAc and tetrahydrofuran (THF), increases the yield slightly (entries 2 and 3). The complete conversion of **1a** was achieved by elongating the reaction time to 120 min, giving **2a** in quantitative yield (entry 4). Eventually, the amount

Table 1 Optimisation of the reaction conditions

Entry	X (atom%)	Y (mol%)	Solvent	Time (min)	Yield of 2a[a] (%)	Yield of 3a[a] (%)
1	0.5	1000	n-hexane	15	58	0
2	0.5	1000	EtOAc	15	62	0
3	0.5	1000	THF	15	64	0
4	0.5	1000	THF	120	99	0
5	0.07	1000	THF	300	99	0
6	0.01	400	THF	300	99	0
7	0.01	200	THF	360	99	0
8	—	200	THF	360	0	0

[a] Determined by GC.

of Au loading could be reduced to 0.01 atom% without a decrease in the yield of **2a**, although a slight extension of the reaction time was required (entries 5–7). The reaction did not proceed in the absence of Au:F-CAC (entry 8). In addition, reducing the amount of water requires a longer reaction time (entries 6 and 7).

Recycling experiments evaluated the durability of the Au:F-CAC catalyst. Fig. 2a presents the result of recycling experiments using 0.01 atom% of Au-F-CAC in THF. The spent catalyst was easily recovered through filtration and reused without additional treatment. Notably, Au:F-CAC exhibited a consistently high activity without substantial loss up to the sixth recycling experiment. The transmission electron microscopy (TEM) images of fresh and reused Au:F-CAC are shown in Fig. 2b. Although slight aggregation of Au nanoparticles was observed after the sixth cycle, the mean diameter of Au NPs was 2.5 ± 1.0 nm, which is within the error of the fresh catalyst (1.7 ± 0.8 nm). The sustained catalytic activity signifies the high stability of this catalyst, likely attributed to the presence of carboxylic acid attached to cellulose. The notable stability of Au:F-CAC allowed us to investigate the size dependency study in this reaction (*vide infra*). The hot filtration of the Au:F-CAC catalyst was conducted to separate the catalyst from the reaction mixture when the yield of **2a** reached 56% (*ca.* after 3 h, Fig. 2c). The resulting filtrate was further treated under the same reaction conditions in the absence of the filtered catalyst, and no increase in the yield of **2a** was observed. In addition, the inductively coupled plasma spectroscopy-atomic emission spectroscopy (ICP-AES) of the filtrate confirmed the absence of Au species (detection limit: 10 ppb). These results indicated that the reaction takes place on the surface of Au nanoparticles in a heterogeneous fashion. Other substrates, such as methyldiphenylsilane (**1b**) and dimethylphenylsilane, were also subjected to the reaction conditions to give the corresponding silanols **2b** and **2c** quantitatively (Table S4†).

Thanks to the high durability of the Au:F-CAC catalyst under the reaction conditions, our attention was then focused
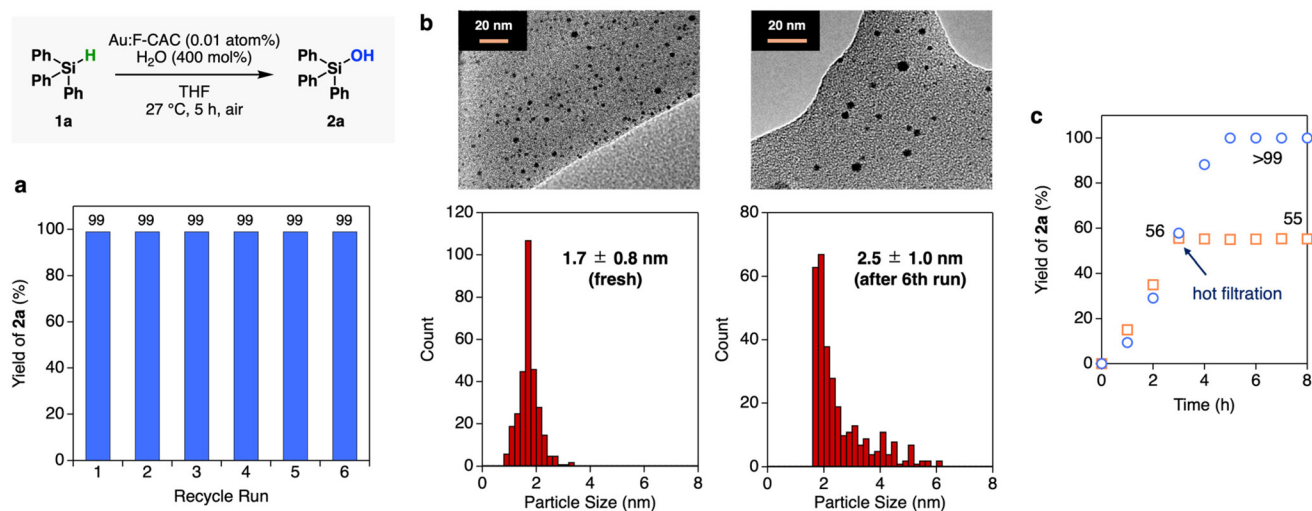
Fig. 2 Catalytic performance of Au-F-CAC catalyst for oxidation of hydrosilane. (a) Recycling run experiment. (b) TEM images of the fresh and spent catalyst after the sixth run. Mean diameter and standard deviation are based on the average 300 particles. (c) Hot filtration experiment.

on the size dependency study. Au:F-CAC catalysts with the sizes of 1.7 ± 0.8 nm, 4.9 ± 0.7 nm, and 7.7 ± 1.4 nm were prepared according to the originally developed *trans*-deposition method for F-CAC,[30] and the kinetic studies were carried out using 0.01 atom% catalysts at 27 °C. In all catalysts, the oxidation reaction proceeded to give **2a**. It should be noted that the severe aggregation of AuNPs was not observed after the reaction, even in the cases of 4.9 nm and 7.7 nm (Fig. S1†). Fig. 3 displays the time-course plots of the concentration of **1a**. The order of the reaction rate was 1.7 nm > 4.9 nm > 7.7 nm. Although the induction period was observed in the case of Au: F-CAC with the size of 7.7 nm (*ca.* 2 h), these plots could be fitted with linear functions, showing the zeroth-order kinetics for **1a**. The zeroth-order kinetics signifies that the catalytically active surface of Au was thoroughly saturated with reactants, which is due to the small amount of Au used ($[\mathbf{1a}]/[N_{\text{surface Au}}] > 14\,000$). Therefore, the zeroth-order kinetic constant (k, mmol L^{-1} h^{-1}) and turnover frequency (TOF) based on total loaded Au

atoms ($\text{TON}_{\text{total Au}}$, h^{-1}) were evaluated using the data after the induction period (Table 2) as follows,

$$\text{TOF}_{\text{total Au}} = \frac{k}{C_{\text{Au}}},$$

where C_{Au} signifies the initial concentration of Au. The $\text{TOF}_{\text{total Au}}$ values of Au:F-CAC of 1.7 nm, 4.9 nm, and 7.7 nm were 3060 h^{-1}, 2160 h^{-1}, and 1200 h^{-1}, respectively. In addition, the TOF based on the surface Au atoms ($\text{TON}_{\text{surface Au}}$) was calculated based on the assumption that AuNPs are spherical with a diameter determined by TEM (d_{TEM}) as follows,

$$\text{TOF}_{\text{surface Au}} = \text{TOF}_{\text{total Au}} \cdot \left(\frac{N_{\text{surface Au}}}{N_{\text{total Au}}} \right)^{-1}$$

$$= \text{TOF}_{\text{total Au}} \cdot \frac{(d_{\text{TEM}})^3}{(d_{\text{TEM}})^3 - (d_{\text{TEM}} - 0.576)^3}$$

The distance between Au atoms in the particles is assumed to be 0.288 nm from the crystal structure of Au. The $\text{TOF}_{\text{surface Au}}$ values of Au:F-CAC of 1.7 nm, 4.9 nm, and 7.7 nm were calculated to be 4304 h^{-1}, 7028 h^{-1}, and 5976 h^{-1}, respectively. These results indicated that Au:F-CAC, with a size of 4.9 nm, exhibited the highest catalytic activity, showing explicit size dependency on the oxidation of hydrosilane. The catalytic activity of previously reported AuNP catalysts, including Au:
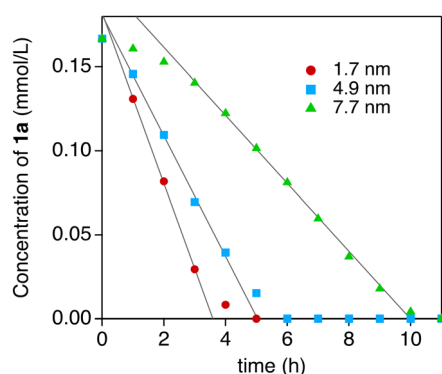

Fig. 3 Plots of the concentration of **1a** after the specific time. The reaction was performed under air using 0.01 atom% Au:F-CAC and H_2O (400 mol%) in THF (3 mL) at 27 °C.

Table 2 Kinetic parameters and catalytic activity

d_{TEM} (nm)	K (mmol L^{-1} h^{-1})	$\text{TOF}_{\text{total Au}}$ [a] (h^{-1})	$\text{TOF}_{\text{surface Au}}$ [b] (h^{-1})
1.7	0.051	3060	4304
4.9	0.036	2160	7028
7.7	0.020	1200	5976

[a] Based on the total Au atoms. [b] Based on the surface Au atoms.

F-CAC, has been compiled in Table S4.† While the catalytic activity, based on TOF, was found to be moderate compared to other catalysts, it is important to note that Au:F-CAC offers distinct advantages. Unlike some alternatives, Au:F-CAC does not necessitate expensive materials or intricate synthetic procedures. In fact, the preparation of F-CAC can be scaled up to 30 grams using straightforward protocols and inexpensive, naturally derived starting materials. This accessibility renders Au:F-CAC a highly convenient nanomaterial option.

The effect of the reaction atmosphere was investigated using 0.01 atom% of Au:F-CAC catalyst at 27 °C and evaluated by the yield of **2a** after 2 h. The yields of **2a** in oxygen, air, and argon atmosphere were 93%, 29%, and 6%, respectively (Table 3). This result clearly indicated that the oxygen partial pressure affects the reaction rate, and the adsorption of molecular oxygen on the surface of Au NP and/or such adsorbed Au species is involved in the rate-determining step. An isotope labelling experiment and theoretical calculations were conducted to understand the reaction mechanism of hydrosilane oxidation. First, the reaction was carried out using $[^{18}O]H_2O$ under ambient aerobic conditions to track the origin of the oxygen atom of silanol.[39] The reaction was completed after 4 h using the optimised reaction conditions. Fourier transform

Table 3 Effect of oxygen partial pressure

Entry	Atmosphere	Yield of **2a**[a] (%)
1	O₂	93
2	Air	29
3	Ar	6

[a] Determined by GC.

infrared (FT-IR) absorption spectroscopy of the thus-synthesized **2a** was measured (Fig. 4a). A peak corresponding to the Si–O vibration appeared at 845 cm⁻¹, red-shifted by 12 cm⁻¹ from that of non-labelled **2a** (857 cm⁻¹). This result indicated the formation of $[^{18}O]$**2a**, and the oxygen atom introduced in **2a** was derived from H_2O rather than molecular oxygen. The theoretical calculations were conducted using the density functional theory (DFT) method at the B3LPY-D3BJ/6-31G(d) level of theory in the gas phase to assign the vibration mode. The Si–¹⁸O vibration was shifted from the Si–¹⁶O vibration by 11 cm⁻¹, showing good agreement with the experimental data (Fig. S4†). Therefore, molecular oxygen accelerates the reaction by adsorbing it on the surface of Au NPs. Previously, we reported that AuNP-catalysed intramolecular cyclisation of amines and/or alcohols proceeded under an aerobic atmosphere using AuNP catalysts, such as Au:PVP[40] and Au:F-CAC.[33] In addition, theoretical calculations were also investigated to suggest that a cationic Au site that catalyses the intramolecular cyclisation was expected to be formed on their surface through the adsorption of molecular oxygens.[41] Given this, the acceleration effect on the oxygen in this reaction would be attributed to the effective formation of the cationic Au species. Camargo et al. reported that the higher number of cationic Au sites formed through Au-support interactions is key for high catalytic activity on the oxidation of hydrosilane, suggesting a good coincidence.[24]

To confirm the formation of cationic Au site experimentally, NAP-XPS experiments were conducted using Au:PVP(K-30, 1.7 nm) as a model catalyst. Au 4f NAP-XPS experiments were conducted at a p_{oxygen} of 0.1 Torr along with ultrahigh vacuum condition (6.8×10^{-9} Torr) using the same sample, where p denotes the partial pressure of gaseous molecules. XP spectra at the Au 4f core level are shown in Fig. 4b. Under ultrahigh vacuum conditions, the peaks corresponding to Au $4f_{7/2}$ and Au $4f_{5/2}$ core levels were observed at 83.7 eV and 87.4 eV, respectively, indicating a shift toward lower binding energy relative to bulk Au (84.0 eV for Au $4f_{7/2}$, 87.7 eV for Au $4f_{5/2}$).[42] This shows the formation of slightly anionic Au(0) species.
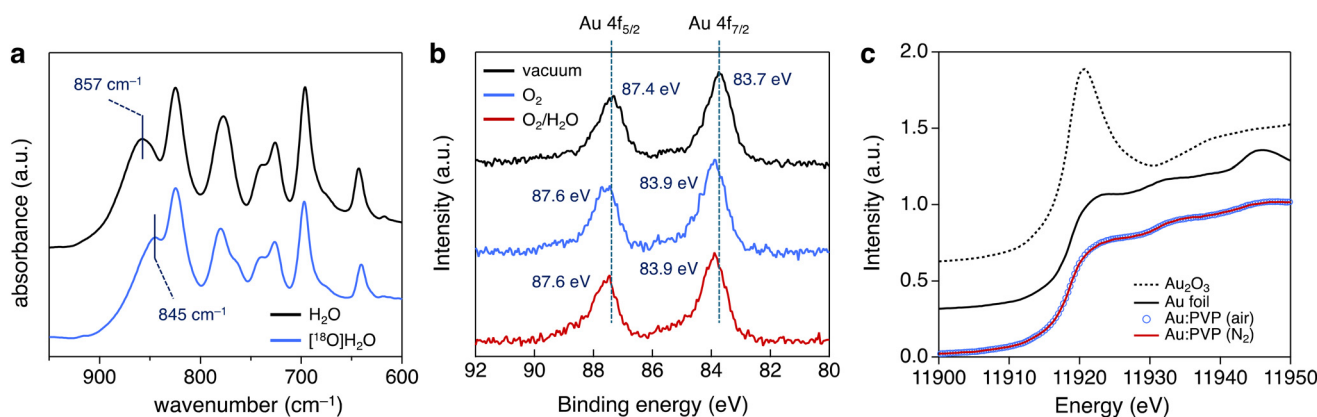

Fig. 4 Mechanistic studies. (a) Isotope labelling experiment using $[^{18}O]H_2O$ and FT-IR spectra of **2a**. Au:F-CAC (0.01 atom%), $[^{18}O]H_2O$ (400 mol%), and THF (3 mL) were used. (b) Au 4f NAP-XPS data of Au:PVP under vacuum (black line), p_{oxygen} = 0.1 Torr (bule line), and p_{oxygen} = 0.1 Torr, p_{H_2O} = 0.1 Torr (red line). (c) Au L_3-edge XAS data of Au:PVP in H_2O.

Meanwhile, Au 4f XPS signals appeared at 83.9 eV and 87.6 eV under the O$_2$ atmosphere (p_{oxygen} = 0.1 Torr). The 0.2 eV shift is attributed to the adsorption of molecular oxygen on the surface of Au NPs, representing experimental evidence for the formation of cationic Au sites. In addition, the NAP-XPS experiment was also conducted under gaseous O$_2$/H$_2$O co-existing condition (p_{oxygen} = 0.1 Torr, p_{water} = 0.1 Torr). However, no further peak shift was observed. These results suggested that molecular oxygen strongly influences the electronic state of AuNPs, while the influence of water is small. To sum up, the NAP-XPS result clearly shows that molecular oxygen plays an essential role in generating active cationic Au sites, explaining the effect of the atmosphere. Hence, this result provides a new aspect of the generally accepted reaction mechanism for the oxidation of hydrosilane.

In addition to the NAP-XPS experiment, the Au L$_3$-edge solution state XAS experiments were also conducted to gain an experimental insight into the electronic state of Au NPs. Au:PVP(K-30) was dissolved in H$_2$O (Au concentration: 8.0 mmol L^{-1}), and the solution was bubbled with N$_2$ gas for 15 min. Then, the solution that was prepared was packed in a gas barrier bag and subjected to the XAS experiment using the fluorescent method. However, the XAS spectra were almost the same before and after bubbling N$_2$ gas due to the existence of a solvent amount of H$_2$O, which adsorbs on the Au surface before the gaseous oxygen (Fig. 4c).

To clarify the detailed mechanism, the kinetic study was further investigated. The reaction rate was plotted against the concentration of H$_2$O, revealing an increase in reaction rate with higher H$_2$O concentration, indicating the participation of H$_2$O in the rate-determining step (RDS) (Fig. S2 and S3†). Next, the reaction rate was measured using D$_2$O as an additive instead of H$_2$O, revealing the presence of a secondary kinetic isotope effect (KIE) (k_H/k_D = 1.17, n = 3), suggesting that the O–H bond cleavage occurs as a pre-equilibrium process before the RDS (Fig. S5†).[43,44] This implies that processes such as dissociative adsorption of H$_2$O or proton transfer are not involved. Based on these experimental findings, a possible reaction mechanism is shown in Fig. 5. The reaction initiates with oxygen adsorption to form cationic Au surface species such as **A**. Subsequently, dissociative adsorption of H$_2$O and hydrosilane occurs through Si–H and/or O–H bond cleavage, yielding intermediate **B** and/or **C**, which exist in equilibrium. Following this, Si–O bond formation is postulated to occur via an S$_N$2 type mechanism, akin to the previously reported PdNP-catalysed dehydrogenative oxidation of hydrosilanes,[45] resulting in the formation of silanol and intermediate **D**. Finally, reductive elimination from **D** occurs on the Au surface to regenerate **A** or **B** with expelling H$_2$ thus completing the catalytic cycle. Although the role of the cationic Au sites generated through the adsorption of O$_2$ remains unclear, further investigations utilizing theoretical calculations are warranted to gain insights into the precise reaction mechanism. It is noteworthy that the actual reaction mechanism is likely more complex than the proposed model mechanism due to the presence of multiple molecules on the surface under experimental conditions.

4. Conclusions

In summary, our study presents the dehydrogenative oxidation of hydrosilane using size-selectively prepared Au:F-CAC catalysts. These catalysts demonstrated notable catalytic activity in terms of TOF and exhibited high stability under the reaction conditions, enabling the exploration of size dependency. Since the first finding of Au NP-catalysed oxidation of hydrosilanes in 2009, the role of oxygen has remained unclear despite its significant influence on reaction facilitation. This study, especially the mechanistic studies, sheds light on a new aspect of the role of oxygen: the formation of cationic Au sites by adsorption. Under such aerobic conditions, it is well known that Au NPs show high catalytic activity in various oxidation reactions, but at the same time, they also possess cationic properties, which is another crucial factor in reaction development and mechanistic studies.

Fig. 5 Possible reaction mechanism.

Author contributions

H. S. and Y. U. conceived and designed the experiments. B. S. performed the preparation and characterizations of catalysts and chemical reactions. Y. U., R. I., R. T., and H. K. performed NAP-XPS experiments and analysis. Y. U. conducted XAS experiments and analysis. B. S. and Y. U. prepared an earlier version of the manuscript, and all authors discussed the results and edited the manuscript.

Conflicts of interest
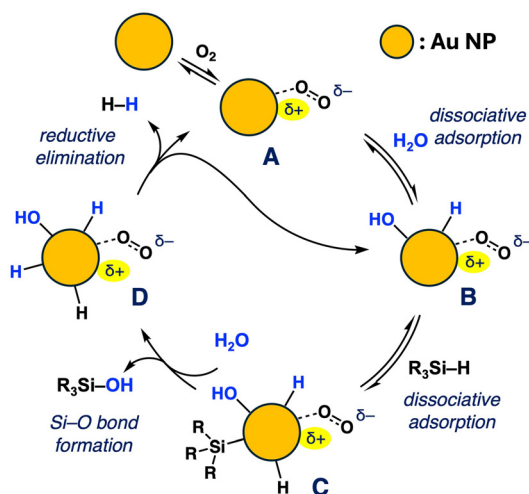
The authors declare no competing interests.

Acknowledgements

References

1 R. Pietschnig, Advances and Properties of Silanol-Based Materials, in *Main Group Strategies towards Functional Hybrid Materials*, 2018, pp. 141–162.

2 A. K. Franz and S. O. Wilson, *J. Med. Chem.*, 2013, **56**, 388.

3 S. E. Denmark and S. Fujimori, *J. Am. Chem. Soc.*, 2005, **127**, 8971.

4 P. W. Long, X. F. Bai, F. Ye, L. Li, Z. Xu, K. F. Yang, Y. M. Cui, Z. J. Zheng and L. W. Xu, *Adv. Synth. Catal.*, 2018, **360**, 2825.

5 M. Jeon, J. Han and J. Park, *ACS Catal.*, 2012, **2**, 1539.

6 P. D. Lickiss and R. Lucas, *J. Organomet. Chem.*, 1996, **521**, 229.

7 K. Valliant-Saunders, E. Gunn, G. R. Shelton, D. A. Hrovat, W. T. Borden and J. M. Mayer, *Inorg. Chem.*, 2007, **46**, 5212.

8 B. Yang and Z. X. Wang, *Org. Lett.*, 2019, **21**, 7965.

9 L. H. Sommer, L. A. Ulland and G. A. Parker, *J. Am. Chem. Soc.*, 1972, **94**, 3469.

10 L. Spialter and J. D. Austin, *J. Am. Chem. Soc.*, 1965, **87**, 4406.

11 J. M. Asensio, D. Bouzouita, P. W. N. M. van Leeuwen and B. Chaudret, *Chem. Rev.*, 2020, **120**, 1042.

12 H. Yamagishi, J. Shimokawa and H. Yorimitsu, *ACS Catal.*, 2023, **13**, 7472.

13 D. Limnios and C. G. Kokotos, *ACS Catal.*, 2013, **3**, 2239.

14 T. Mitsudome, A. Noujima, T. Mizugaki, K. Jitsukawa and K. Kaneda, *ChemComm*, 2009, 5302.

15 T. Urayama, T. Mitsudome, Z. Maeno, T. Mizugaki, K. Jitsukawa and K. Kaneda, *Chem. Lett.*, 2015, **44**, 1062.

16 L. Ma, W. Leng, Y. Zhao, Y. Gao and H. Duan, *RSC Adv.*, 2014, **4**, 6807.

17 T. Mitsudome, Y. Yamamoto, A. Noujima, T. Mizugaki, K. Jitsukawa and K. Kaneda, *Chem. – Eur. J.*, 2013, **19**, 14398.

18 N. Asao, Y. Ishikawa, N. Hatakeyama, Menggenbateer, Y. Yamamoto, M. Chen, W. Zhang and A. Inoue, *Angew. Chem., Int. Ed.*, 2010, **49**, 10093.

19 V. Gitis, R. Beerthuis, N. R. Shiju and G. Rothenberg, *Catal. Sci. Technol.*, 2014, **4**, 2156.

20 T. Liu, F. Yang, Y. Li, L. Ren, L. Zhang, K. Xu, X. Wang, C. Xu and J. Gao, *J. Mater. Chem.*, 2014, **2**, 245–250.

21 G. M. A. Rahman, D. M. Guldi, E. Zambon, L. Pasquato, N. Tagmatarchis and M. Prato, *J. Nanotechnol.*, 2005, **1**, 527.

22 J. John, E. Gravel, A. Hagège, H. Li, T. Gacoin, T. Gacoin and E. Doris, *Angew. Chem., Int. Ed.*, 2011, **50**, 7533.

23 Z. T. Xie, T. Asoh, Y. Uetake, H. Sakurai and H. Uyama, *Carbohydr. Polym.*, 2020, **247**, 116723.

24 A. G. M. da Silva, C. M. Kisukuri, T. S. Rodrigues, E. G. Candido, I. C. de Freitas, A. H. M. da Silva, J. M. Assaf, D. C. Oliveira, L. H. Andrade and P. H. C. Camargo, *Appl. Catal.*, 2016, **184**, 35.

25 H. T. Tang, H. Y. Zhou, Y. M. Pan, J. L. Zhang, F. H. Cui, W. H. Li and D. Wang, *Angew. Chem., Int. Ed.*, 2024, **63**, e202315032.

26 X. Cui, A. Ozaki, T. Asoh and H. Uyama, *Polym. Degrad. Stab.*, 2020, **175**, 109118.

27 X. Cui, T. Honda, T. Asoh and H. Uyama, *Carbohydr. Polym.*, 2020, **230**, 115662.

28 S. Haesuwannakij, T. Poonsawat, M. Noikham, E. Somsook, Y. Yakiyama, R. N. Dhital and H. Sakurai, *J. Nanosci. Nanotechnol.*, 2017, **17**, 4649.

29 S. Haesuwannakij, Y. Yakiyama and H. Sakurai, *ACS Catal.*, 2017, **7**, 2998.

30 T. Chutimasakul, Y. Uetake, J. Tantirungrotechai, T. Asoh, H. Uyama and H. Sakurai, *ACS Omega*, 2020, **5**, 33206.

31 H. Tsunoyama, H. Sakurai, Y. Negishi and T. Tsukuda, *J. Am. Chem. Soc.*, 2005, **127**, 9374.

32 H. Tsunoyama, H. Sakurai and T. Tsukuda, *Chem. Phys. Lett.*, 2006, **429**, 528.

33 Y. Uetake, B. Suwattananuruk and H. Sakurai, *Sci. Rep.*, 2022, **12**, 20602.

34 S. Sasaki, K. Kakuno, T. Takada, T. Shimada, K. Yanagida and Y. Miyahara, *Nucl. Instrum. Methods Phys. Res., Sect. A*, 1993, **331**, 763.

35 K. Amemiya and T. Ohta, *J. Synchrotron Radiat.*, 2004, **11**, 171.

36 J. J. Rehr and R. C. Albers, *Rev. Mod. Phys.*, 2000, **72**, 621.

37 M. Newville, *J. Synchrotron Radiat.*, 2001, **8**, 322.

38 B. Ravel and M. Newville, *J. Synchrotron Radiat.*, 2005, **12**, 537.

39 Q. Zhang, M. Peng, Z. Gao, W. Guo, Z. Sun, Y. Zhao, W. Zhou, M. Wang, B. Mei, X. L. Du, Z. Jiang, W. Sun, C. Liu, Y. Zhu, Y. M. Liu, H. Y. He, Z. H. Li, D. Ma and Y. Cao, *J. Am. Chem. Soc.*, 2023, **145**, 4166.

40 H. Kitahara and H. Sakurai, *Chem. Lett.*, 2009, **39**, 46.

41 K. Bobuatong, H. Sakurai and M. Ehara, *ChemCatChem*, 2017, **9**, 4450.

42 H. Tsunoyama, N. Ichikuni, H. Sakurai and T. Tsukuda, *J. Am. Chem. Soc.*, 2009, **131**, 7086.

43 E. M. Simmons and J. F. Hartwig, *Angew. Chem., Int. Ed.*, 2012, **51**, 3066.

44 N. J. F. Christensen, *Synlett*, 2015, 508.

45 T. Kamachi, K. Shimizu, D. Yoshihiro, K. Igawa, K. Tomooka and K. Yoshizawa, *J. Phys. Chem. C*, 2013, **117**, 22967.